Acta Mech. Sin. (2016) 32(3):406–421
DOI 10.1007/s10409-015-0554-y

RESEARCH PAPER

Process, mechanism and impacts of scale formation in alkaline flooding by a variable porosity and permeability model

Zhen Zhang[1] · **Jiachun Li**[1]

Received: 9 October 2015 / Revised: 2 December 2015 / Accepted: 9 December 2015 / Published online: 10 March 2016

Abstract In spite of the role of alkali in enhancing oil recovery (EOR), the formation of precipitation during alkaline-surfactant-polymer (ASP) flooding can severely do harm to the stratum of oil reservoirs, which has been observed in situ tests of oil fields such as scale deposits found in oil stratum and at the bottom of oil wells. On the other hand, remarkable variation of stratum parameters, e.g., pore radius, porosity, and permeability due to scale formation considerably affects seepage flow and alkaline flooding process in return. The objective of this study is to firstly examine these mutual influential phenomena and corresponding mechanisms along with EOR during alkaline flooding when the effects of precipitation are no longer negligible. The chemical kinetic theory is applied for the specific fundamental reactions to describe the process of rock dissolution in silica-based reservoirs. The solubility product principle is used to analyze the mechanism of alkali scale formation in flooding. Then a 3D alkaline flooding coupling model accounting for the variation of porosity and permeability is established to quantitatively estimate the impact of alkali scales on reservoir stratum. The reliability of the present model is verified in comparison with indoor experiments and field tests of the Daqing oil field. Then, the numerical simulations on a 1/4 well group in a 5-spot pattern show that the precipitation grows with alkali concentration, temperature, and injection pressure and, thus, reduces reservoir permeability and oil recovery correspondingly. As a result, the selection of alkali with a weak base is preferable in ASP flooding by tradeoff strategy.

Keywords Alkali · Precipitation · Chemical flood · Permeability · Oil recovery

1 Introduction

In China, 60%–70% of crude oil was still trapped in the reservoirs after water flooding and chemical reagents, i.e., polymer, surfactant, and microorganisms were again injected into the reservoir to increase the oil production [1–4]. Among them, alkaline flooding is one of the enhance oil recovery (EOR) techniques, in which alkaline chemicals, such as sodium orthosilicate (Na_4SiO_4), sodium carbonate (Na_2CO_3), or sodium hydroxide (NaOH) are mixed into the injected water. The use of alkaline chemicals to enhance oil recovery has been widely documented [5,6]. The injected alkaline agents then react with the acidic species contained in the crude oils to produce surface-active soap species for reducing the interfacial tension (IFT) by several orders of magnitude to ultra-low values [7]. It is the dominant mechanism for caustic water-flooding to improve oil recovery.

In spite of the role of alkali in EOR, the formation of precipitation during chemical flooding may severely do harm to oil reservoirs. Alkali agents can react with reservoir rock to produce alkali scales, which have been observed in many oil field tests. In this regard, Efremov and Vachourkine [8] reported the precipitation of calcium and magnesium carbonates in a field test in the Western Siberia–Trekhozernoye field of Russia. In addition, Krumrine et al. [9] analyzed the scale formation at the Long Beach Unit Pilot and found that

✉ Jiachun Li
jcli05@imech.ac.cn

[1] Key Laboratory of Mechanics in Fluid Solid Coupling Systems, Institute of Mechanics, Chinese Academy of Sciences, Beijing 100190, China

the scales formed in producing wells were made up of calcium carbonate, magnesium silicate, and silicate scales. Scale deposit was reported in the Daqing Oilfield during alkaline-surfactant-polymer (ASP) flooding by Li et al. [10] and Zhao et al. [11]. Song et al. [12] examined the scaling characteristics of ASP in multi-well groups and found that larger well space would result in serious scaling. Also, Joseph et al. [13] mentioned severe silicate scale occurring at a production well of an oilfield in southern Alberta, which led to laborious well work-over such as pumps and associated rod replacement.

Some authors have studied the formation of scales through laboratory experiments. Liu et al. [14] investigated the precipitation of alum silicates on Kaolinite by X-ray diffraction. Additional studies by Abu-Khamsin and Ahmad [15] showed the scaling of calcium sulphate in Berea sandstone cores in the laboratory and analyzed the effects of pressure, temperature, and flow rate on the deposition of calcium sulphate. It was observed by Amer [16] that there was permeability reduction due to the precipitation of calcium, barium, and strontium sulfates in sandstone cores. Zhang and Chen [17] analyzed the representative scaling sample from ASP flooding in the Daqing oil field and analyzed the scaling rules.

A few studies in the literature on the influence of chemical reactions on the reservoir parameters are found. This phenomenon is commonly observed over a geological period of time [18–21]. In contrast, the oil exploitation process is relatively transitory. A few researchers started to notice the effects of alkaline scales on stratum parameters through laboratorial instruments [22,23]. For instance, Cheng [24] observed the influence of different kinds of alkali on the permeability through indoor experiments. Also, Li et al. [10] used drops infiltration experiments to analyze the variation of permeability and porosity.

With a great many chemical reactions involved, numerical simulation of alkaline flooding seems to be very complicated [25,26]. A model based on the fractional-flow theory was developed by Ramakrishnan and Wasan [27] to simulate high-pH processes, only considering the interaction between oil and alkaline agents. In additon, Bhuyan et al. [28] combined the detailed reaction chemistry like oil/alkali chemistry, ion exchange, precipitation, and flow properties in alkaline flooding, while the rock dissolution was neglected. Labrid and Pierre [29] also studied the migration of alkali in the chemical displacement process with alkali/rock reactions such as ion exchange and rock dissolution taken into account. A predictive model for silica scaling was established by Li et al. [10] according to the solubility product theory and applied the model to quantitatively predict the silica scaling in the test site of Xingbei Oilfield of the Daqing area. The dissipative particle dynamics (DPD) method was applied to study the physicochemical hydrodynamics at the pore scale and verified the accuracy of the DPD simulation using the plane Poiseuille flow [30].

Due to the harmful effects of alkaline scales, it is essential to carry out a qualitative assessment of the reservoir parameters (especially the porosity and permeability) prior to the large-scale exploitation of an oil-field. During the injection of alkaline solutions with alkaline-rock interactions, the reservoir parameters will be impacted. Previous alkaline flood models only considered increasing silicate ion concentration due to the dissolution of reservoir rock during the flooding process, neglecting the impact of alkali scales on the stratum parameters. Although several studies in the literature dealt with the mechanism of precipitation and got the permeability reduction information in laboratories, few people quantitatively studied the effect of scaling on the permeability and porosity by numerical simulation.

In this study, we consider major physicochemical phenomena (such as alkali/oil reactions, ion-exchange, rock dissolution, precipitation, alkali loss, and residual oil). In particular, a coupling model of variable porosity and permeability is put forward to examine these mutual influential phenomena and corresponding mechanisms during the processes. The article consists of the following parts: Firstly, the theory of rock dissolution and precipitation of new minerals is briefly elaborated. Next, a displacement model for a silica-based reservoir is presented for an alkaline flooding study based on a finite difference method (FDM) scheme. Verified by comparing calculated results with field tests and laboratory experiments, the model is then used to explore the physicochemical process, focusing on the mechanism and impact of rock dissolution and scale formation on the stratum.

2 The variation of porosity and permeability for silica-based reservoirs

2.1 Rock dissolution in alkaline flooding

The precipitation and production of alkali scales are certainly dependent on the mineral composition of rocks such as silicates, alumina, carbonate and sulfates. This study is only restricted to the rocks of the Daqing oil-field, which is a silica-based reservoir and the main components include quartz, feldspars, and clays.

Since quartz consisting of SiO_2 is the main constituent of rock in many reservoirs, we begin by examining the process of dissolution of SiO_2 in more detail. The quartz dissolution at pH 7 can be expressed as Eq. (1a). When the pH is greater than 7, H_4SiO_4 becomes ionized, expressed in Eq. (1b) and Eq. (1c) [31].

$$SiO_2(s) + 2H_2O \rightleftharpoons H_4SiO_4, \tag{1a}$$

Table 1 Chemical equilibria in alkaline flooding

Reactions	Equilibrium constant definition	Value
$HA_o \rightleftharpoons HA_w$	$k_D = \frac{[HA_o]}{[HA_w]}$	1.0×10^4 (Ref. [25])
$HA_w \rightleftharpoons A^- + H^+$	$k_A = \frac{[H^+][A^-]}{[HA_w]}$	1.0×10^{-10} (Ref. [25])
$H_2O \rightleftharpoons H^+ + OH^-$	$k_w = [H^+][OH^-]$	1.0×10^{-14} (Ref. [25])
$SiO_2\,(\text{amorphous}) + 2H_2O \rightleftharpoons H_4SiO_4$	$k_3^{eq} = \left[H_2SiO_4^{2-}\right]^{sat}$	2.0×10^{-3} (Ref. [31])
$H_4SiO_4 + OH^- \rightleftharpoons H_3SiO_4^- + H_2O$	$k_4^{eq} = \frac{[H_3SiO_4^-]}{\left[H_2SiO_4^{2-}\right][OH^-]}$	4940 (Ref. [31])
$H_3SiO_4^- + OH^- \rightleftharpoons H_2SiO_4^{2-} + H_2O$	$k_5^{eq} = \frac{\left[H_2SiO_4^{2-}\right]}{[H_3SiO_4^-][OH^-]}$	2.4 (Ref. [31])
$\bar{H}^+ + Na^+ \rightleftharpoons \bar{N}a^+ + H^+$	$k_1^{ex} = \frac{[\bar{H}^+][Na^+]}{[H^+][\bar{N}a^+]}$	0.18 (Ref. [35])
$2Na^+ + \bar{C}a^{2+} \rightleftharpoons 2\bar{N}a^+ + Ca^{2+}$	$k_2^{ex} = \frac{[Ca^{2+}][\bar{N}a^+]^2}{[\bar{C}a^{2+}][Na^+]^2}$	0.2564 (Ref. [36])
$Ca\,(OH)_2 \rightleftharpoons Ca^{2+} + 2OH^-$	$k_1^{sp} = [Ca^{2+}][OH^-]^2$	$f\,(T)$
$Q_v = 2\bar{C}a + \bar{N}a + \bar{H}$		$f\,(\text{pH})$
$[Si] = \left[H_2SiO_4^{2-}\right] + \left[H_3SiO_4^-\right] + \left[H_2SiO_4^{2-}\right]$		$f\,(\text{pH})$

$$H_4SiO_4 + OH^- \rightleftharpoons H_3SiO_4^- + H_2O, \tag{1b}$$

$$H_3SiO_4^- + OH^- \rightleftharpoons H_2SiO_4^{2-} + H_2O. \tag{1c}$$

Based on O'Connor and Greenberg's disassion [32], the rate of SiO_2 dissolution looks like

$$r = \frac{dC_{Si}}{dt} = k_1 A - k_2 C_{Si} A, \tag{2}$$

where r denotes reaction rate, C_{Si} the concentration of amorphous silica, t the time, k_1 the dissolution rate constant, k_2 the condensation rate constant, and A is surface area.

The solution of Eq. (2) can be written as

$$C_{Si} = C_{sat}^{Si}(1 - e^{-kt}), \tag{3}$$

where k is the equilibrium constant. C_{sat}^{Si} is the saturated concentration of silicon dependent on the value of pH.

The mass conservation equation of silicon element reads:

$$[Si] = [H_4SiO_4] + \left[H_3SiO_4^-\right] + \left[H_2SiO_4^{2-}\right]. \tag{4}$$

According to the definition of the equilibrium constant, shown in Table 1, the concentration of $H_3SiO_4^-$, $H_2SiO_4^{2-}$ can be written as $\left[H_3SiO_4^-\right] = k_4^{eq}[H_4SiO_4][OH^-]$, $\left[H_2SiO_4^{2-}\right] = k_4^{eq}k_5^{eq}[H_4SiO_4][OH^-]^2$.

If the concentrations are expressed in terms of the equilibrium constants and the concentration of hydroxide ion in solution is OH^-, then

$$[Si] = \left[H_2SiO_4^{2-}\right]\left(1 + k_4^{eq}[OH^-] + k_4^{eq}k_5^{eq}[OH^-]^2\right). \tag{5}$$

2.2 Scale precipitation formation

Usually there are three types of alkali scales: carbonate scales, hydroxide precipitates, and silicate precipitates. The analytical results on some scaling samples collected in the Daqing field show that the main components include amorphous SiO_2, kaolinite, and hydroxide precipitates.

In this paper, the solubility product principle is used to depict the formation of scales. Hydroxide precipitates are a direct result of increasing pH in an alkaline flood. As an example, we take calcium hydroxide to illustrate the solubility product principle

$$Ca^{2+} + 2OH^- \rightleftharpoons Ca\,(OH)_2\,(s). \tag{6}$$

The equilibrium solubility of calcium hydroxide can be written as

$$J = [Ca^{2+}][OH^-]^2, \tag{7}$$

where J is the ion product and the brackets denote solution concentration in molar units. K_{sp} is the solubility product constant reflecting the solubility of insoluble material. The solubility product constant varies with temperature.

If $J = K_{sp}$, it means that the solution is saturated and reaches a dynamic equilibrium state. No precipitation exists in the solutions. If $J < K_{sp}$, the solution is unsaturated. There is no precipitation in the solution. If $J > K_{sp}$, the solution

is supersaturated and crystallization may occur. With concentration less than 10^{-5} mol/L, a completely precipitated cation is implied.

2.3 Variable permeability and porosity model

Due to its simple application, the Kozeny-Carman (KC) model [33,34] is widely used to describe the permeability-porosity relationship.

Our approach is to yield a simpler macroscopic model of permeability according to the basic KC equation. The real seepage flow is given by Darcy's law. On the assumption that real porous media is regarded as a tortuous isodiametric capillary tube, as shown in Fig. 1, the Poiseuille formula is used to describe the fluid flow. Then the permeability is expressed as

$$K = \frac{\phi r^2}{8\tau^2}. \tag{8}$$

This expression of permeability is good for unconsolidated media and here the new precipitation is unconsolidated. Then we take calcium hydroxide as an example to demonstrate the variation of porosity and permeability due to scale precipitation in the alkaline flooding.

When no precipitation occurs, the pore volume of a calculated cell can be expressed as

$$V_1 = \Delta x \Delta y \Delta z \phi_1. \tag{9}$$

Assume the concentration of generated scaling $Ca(OH)_2$ is C mol/L. The volume of generated scaling is

$$V_{\text{scale}} = \frac{C \Delta x \Delta y \Delta z \phi_1 M 10^{-3}}{\rho}, \tag{10}$$

where M and ρ are the molar mass and density of $Ca(OH)_2$, respectively. If the precipitation occurs, the pore volume of a calculated cell is reduced to $V_2 = V_1 - V_{\text{scale}}$.

Then the new porosity of a reservoir becomes

$$\phi_2 = \frac{V_2}{\Delta x \Delta y \Delta z} = \phi_1 \left(1 - \frac{10^{-3} C M}{\rho}\right). \tag{11}$$

With the aim of explaining the influence of the formation of precipitation on the pore radius in the stratum, we assume the pore channels are cylindrical with constant length. In this way, the new pore radius can be written as

$$r_2 = \sqrt{\frac{V_2}{V_1}} r_1, \tag{12}$$

where V is the pore volume. Subscripts 1, 2 indicate pre-precipitation and post-precipitation. The new permeability of a reservoir can be expressed as $K_2 = \frac{\phi_2 r_2^2}{8\tau^2}$.

3 Mathematical formulation of alkaline flooding

3.1 Phase transport model

3.1.1 Assumption

Since numerous complicated chemical reactions are involved in alkaline flooding, a comprehensive model should be so elaborated as to describe the major process of alkali transport in porous media based on the following assumptions:

(1) Solid phase is basically stationary.
(2) All phases are in equilibrium state everywhere.
(3) The reservoir is assumed to be isothermal.
(4) Thermodynamic equilibrium is attained for chemical reactions in the liquid phase for ionic exchange.
(5) Both fluids and reservoir rock are assumed compressible.

Please note that all ion concentrations are expressed in moles per liter of aqueous phase and adsorbed cations are distinguished from cations in solution by overbars.

3.1.2 Mass conversation law

The oil and water phase mass balance equations are:

$$\frac{\partial (\phi S_o \rho_o)}{\partial t} = \nabla \cdot \left[\frac{\rho_o K K_{ro}}{\mu_o} \nabla (p_o + \rho_o g \Delta z)\right] + q_o, \tag{13}$$

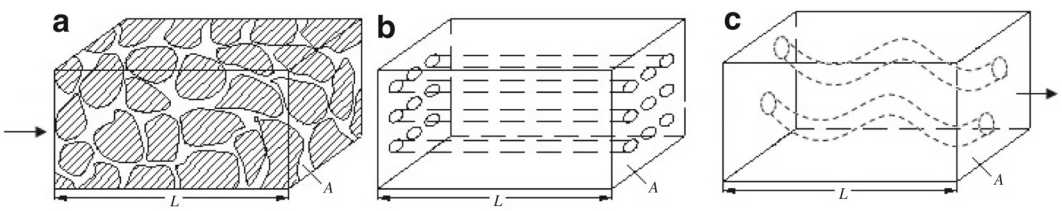

Fig. 1 Sketch of capillary tube model. **a** Real porous media. **b** Isodiametric capillary tube. **c** Tortuous isodiametric capillary tube

$$\frac{\partial(\phi S_a \rho_a)}{\partial t} = \nabla \cdot \left[\frac{\rho_a K K_{ra}}{\mu_a} \nabla (p_a + \rho_a g \Delta z) \right] + q_a, \quad (14)$$

where K, p, ρ, μ, S denote effective permeability, pressure, density, viscosity, and saturation. q is source or sink terms. Subscripts a, o represent aqueous and oleic phases, respectively.

The saturation relation

$$S_o + S_a = 1 \quad (15)$$

should be satisfied. The capillary force equation:

$$p_c = p_o - p_a = \sigma \cos\theta \sqrt{\varphi / K} J(S_a), \quad (16)$$

where p_c is the capillary force, and $J(S_a)$ is the capillary force function. σ, θ is the IFT and contact angle between oleic and aqueous phases.

3.1.3 Coupled reaction-transport model

As shown in Table 2, there are 14 variables in alkaline solutions. Considering the chemical equilibrium equations, listed in Table 1, we only include three dependent variables' hydrodynamic conservation equations in the model.

Sodium, with the ion-exchange:

$$\begin{aligned} &\frac{\partial(\phi S_a \rho_a C_{Na})}{\partial t} + \frac{\partial\left(\phi S_a \rho_a C_{\overline{Na}}\right)}{\partial t} \\ &= \nabla \cdot [D \phi S_a \nabla (C_{Na} \rho_a)] \\ &\quad + \nabla \cdot \left[C_{Na} \frac{\rho_a K K_{ra}}{\mu_a} \nabla (p_a + \rho_a g \Delta z) \right] + q_a C_{injNa}. \end{aligned} \quad (17)$$

Calcium, including the ion-exchange and precipitation:

$$\begin{aligned} &\frac{\partial(\phi S_a \rho_a C_{Ca})}{\partial t} + \frac{\partial\left(\phi S_a \rho_a C_{\overline{Ca}}\right)}{\partial t} + \frac{\partial\left(\phi S_a \rho_a C_{Ca_s}\right)}{\partial t} \\ &= \nabla \cdot [D \phi S_a \nabla (C_{Ca} \rho_a)] \\ &\quad + \nabla \cdot \left[C_{Ca} \frac{\rho_a K K_{ra}}{\mu_a} \nabla \left(p_a + \rho_{ag} \Delta z\right) \right] + q_a C_{injCa}. \end{aligned} \quad (18)$$

Table 2 Reactive elements and chemical species in alkaline flooding

	Chemical species
Independent species	OH^-, Na^+, Ca^{2+}
Dependent species	H^+, HA_w, HA_o, A^-, $H_3SiO_4^-$, $H_2SiO_4^{2-}$, H_4SiO_4
Solid species	$Ca(OH)_2(s)$
Rock-adsorbed cations	$\bar{H}^+$, $\bar{N}a^+$, $\bar{C}a^{2+}$

Hydroxide, considering the alkali loss:

$$\begin{aligned} &\frac{\partial(\phi S_a \rho_a C_{OH})}{\partial t} = \nabla \cdot [D \phi S_a \nabla (C_{OH} \rho_a)] \\ &\quad + \nabla \cdot \left[C_{OH} \frac{\rho_a K K_{ra}}{\mu_a} \nabla (p_a + \rho_a g \Delta z) \right] \\ &\quad + q_a C_{injOH} + R_{OH}, \end{aligned} \quad (19)$$

where D is the dispersion coefficient. C is the concentration of the chemical element. The state equations:

$$\rho_o = \rho_{o0} [1 + C_o (p_o + \rho_o g z - p_{o0})], \quad (20)$$

$$\rho_a = \rho_{a0} [1 + C_w (p_a + \rho_a g z - p_{a0})], \quad (21)$$

$$\phi = \phi_0 \left[1 + C_\phi \left(\frac{p_a + p_o + \rho_o g z + \rho_a g z}{2} - \frac{p_{a0} + p_{o0}}{2} \right) \right], \quad (22)$$

in which C_ϕ, C_a, and C_o are the compressibility of rock, water, and oil, respectively. Subscript 0 indicates parameter values at a certain condition.

3.2 Description of physico-chemical phenomena

3.2.1 Variation of IFT with pH value

In caustic flooding, the IFT is related to the type and concentration of alkali. A relation between IFT and pH value is given according to the experimental data of the Daqing oil-field, as shown in Fig. 2.

3.2.2 In-situ surfactant

The concentration of in-situ surfactant A^- can be derived according to the mass conservation of active acid HA, which distributes itself between the oleic and the aqueous phases

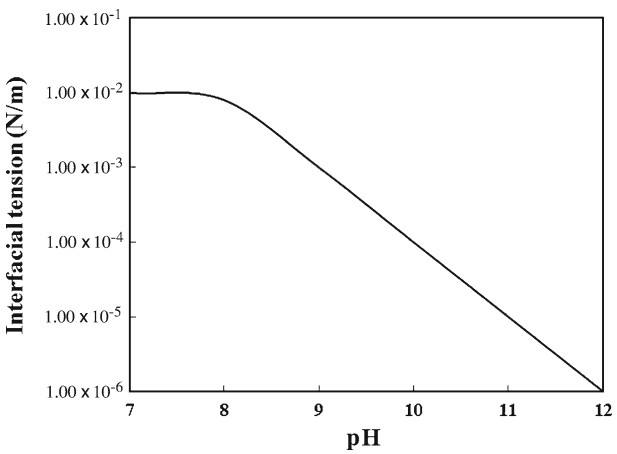

Fig. 2 Relationship between IFT and pH

in a constant distribution ratio, before and after the reaction, shown in Eq. (23).

$$S_o C_{HA_o} + S_w \left(C_{HA_w} + C_{A^-}\right) = S'_o C'_{HA_o} + S'_w \left(C'_{HA_w} + C'_{A^-}\right). \tag{23}$$

Based on the definition of the distribution coefficient of active acid $k_D = \frac{[HA_o]}{[HA_w]}$, dissociation equilibrium of active acid $k_A = \frac{[H^+][A^-]}{[HA_w]}$, and dissociation equilibrium of water $k_w = [H^+][OH^-]$, the concentration of A^- after the chemical reaction is:

$$C'_{A^-} = \frac{S_o C_{HA_o} + S_w \left(C_{HA_w} + C_{A^-}\right)}{S'_w \left(\frac{K_D K_w}{K_A C^-_{OH}} + \frac{K_w}{K_A C^-_{OH}} + 1\right)}. \tag{24}$$

3.2.3 Residual oil saturation

The residual oil saturation may be expressed as a function of in-situ produced surfactant written as [25]

$$S_{or} = a_1 + a_2 \exp\left(-\frac{C_{A^-}}{a_3}\right). \tag{25}$$

3.2.4 Relative permeability

Relative permeability curves suggested by Larson and Hirasaki [37] are used here.

$$K_{ro} = K^0_{ro}\left(\frac{S_o - S_{or}}{1 - S_{wc} - S_{or}}\right)^{e_o},$$
$$K_{ra} = K^0_{ra}\left(\frac{S_a - S_{wc}}{1 - S_{wc} - S_{or}}\right)^{e_a}, \tag{26}$$

where K_{ro} and K_{ra} are relative permeability of aqueous and oleic phases, respectively. S_{wc} and S_{or} connate water saturation and residual oil saturation. K^0_{ra} and K^0_{ro} are relative permeability of the aqueous phase at residual oil saturation, and relative permeability of oil at connate water saturation. e_a and e_o are the exponent in aqueous relative permeability relation and the exponent in oleic relative permeability relation, respectively.

K^0_{ra}, K^0_{ro}, e_a, e_o, S_{wc} vary with the IFT and are regarded as a function of IFT. We give two sets of relative permeability curves in extreme situations, as shown in Table 3 [38].

Table 3 Residual saturation and relative permeability

IFT (N/m)	K^0_{ra}	K^0_{ro}	S_{wc}	e_a	e_o
0.01	0.11	0.53	0.2	1.5	2
0.0001	0.75	0.9	0.07	1.0	1.9

3.2.5 Ion exchange

When the alkaline solution is injected into the reservoir, the new added ions have the priority of adsorption over the ions. The ion exchanges of sodium/hydrogen and sodium/calcium are the main ion-exchange reactions described as

$$M\bar{H}^+ + Na^+ \rightleftharpoons M\bar{N}a^+ + H^+, \tag{27}$$
$$2Na^+ + M_2\bar{C}a^{2+} \rightleftharpoons 2M\bar{N}a^+ + Ca^{2+}. \tag{28}$$

The adsorbed sodium can be expressed by the Langmuir equilibrium adsorption isotherm [39].

$$C_{\bar{N}a} = \frac{aC_{Na}}{1 + bC_{Na}}, \tag{29}$$

where M denotes a mineral exchange site. a, b is the equilibrium adsorption constant.

$$Q_v = 2\bar{C}a + \bar{N}a + \bar{H}. \tag{30}$$

All the cations adsorbed on the rock surface equal the cation exchange capacity (CEC). The CEC can be defined as [36]

$$Q_v = Q_1 + Q_2 \frac{k_{ec} C^-_{OH}}{1 + k_{ec} C^-_{OH}}, \tag{31}$$

in which k_{ec} is the equilibrium constant.

3.2.6 Alkali loss (hydroxide loss)

Alkali loss is a very important phenomenon in alkaline flooding. Four influential factors relevant for alkali consumption are involved in the present model.

$$R^-_{OH} = -\phi \rho_a S_a \frac{\partial}{\partial t}\left(r_1 + r_2 + r_3 + r_4\right), \tag{32}$$

r_1, r_2, r_3, and r_4 represent the alkali loss caused by the reactions between alkaline and acidic species of crude oil, ion exchange, the OH^-, and the rock dissolution.

3.3 Solving process

The whole solution procedure is described as follows.

(1) Find the physico-chemical parameters such as the density, viscosity, interfacial tension, residual oil saturation, capillary force, etc. at first according to the initial conditions and chemical reaction equations.
(2) Solve for the pressure and saturation of the oleic phase and the aqueous phase with Eqs. (13) and (14) by the implicit pressure and explicit saturation (IPES) method.

(3) Calculate the flow rate of each phase according to the Darcy Law.
(4) Compute the concentration of each element with Eqs. (17), (18), and (19) under the pressure and saturation obtained in the previous step and then consider the variation of porosity and permeability.

4 Verification of the variable porosity and permeability model

In order to verify the established flooding model accounting for precipitation, we have compared the simulated results with laboratory experiments and field tests.

4.1 Verification 1

In the lab, Amer [16] prepared sandstone cores of 1 inch (1 inch = 2.54 cm) in diameter and 3 inches in length with porosity of 32 % and permeability of 13.1 md, on average, from Malaysia to examine the permeability reduction owing to the deposition of calcium, strontium, and barium sulfates by injecting mixed sea water and formation water containing a high concentration of calcium, strontium, and barium ions at various temperatures (50 °C − 80 °C) and different pressures (100–200 psi). The deposition of scales was observed by scanning electron microscopy (SEM) micrographs.

Based on the precipitation model in this study, we can also derive the permeability reduction under the same conditions. Then, the permeability ratio (PR) is used to measure the degree of permeability reduction given by:

$$PR = \frac{K_p}{K_i} = \frac{\text{Permeability after precipitation}}{\text{Initial permeability}}. \tag{33}$$

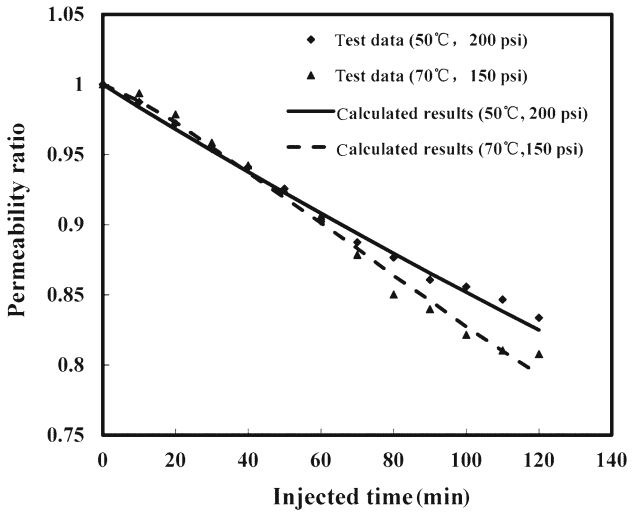

Fig. 3 Comparison between core test data and calculated results on the permeability ratio (*diamond dot* represent the results at temperature 50 °C and pressure 200 psi; *triangle* represent the results at temperature 70 °C, and pressure 150 psi; *solid line* is the calculated results at temperature 50 °C and pressure 200 psi; *dashed line* is the calculated results at temperature 70 °C and pressure 150 psi; core test data come from Ref. [16])

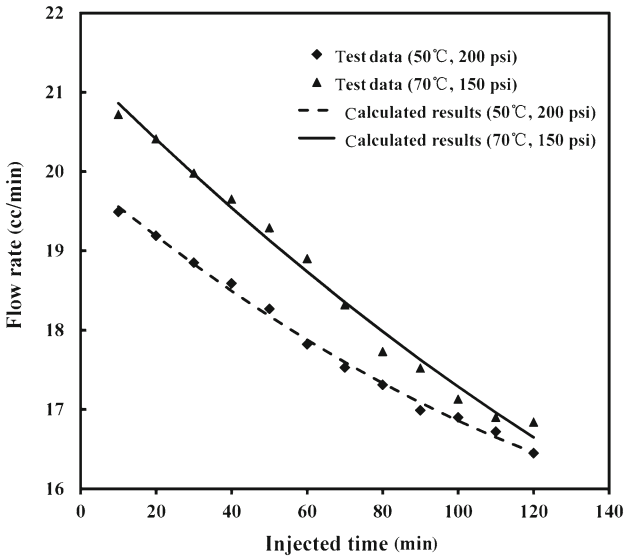

Fig. 4 Comparison between core test data and calculated results on flow rate (*diamond dot* represent the results at temperature 50 °C and pressure 200 psi; *triangle* represent the results at temperature 70 °C and pressure 150 psi; *dashed line* is the calculated results at temperature 50 °C and pressure 200 psi; *solid line* is the calculated results at temperature 70 °C and pressure 150 psi; core test data come from Ref. [16])

Figures 3 and 4 show the variation of permeability ratio and flow rate at different conditions. It is seen that the permeability and flow rate is affected by temperature and pressure, which will be further discussed in the following section. It is also evident that the permeability diminishes with the formation of precipitation in the displacement process. For example, if the temperature is 70 °C and pressure is 150 psi, the permeability ratio is 0.94 when the injected time is 40 min. With the flooding going on for 80 min, the permeability ratio further lessens to 0.85, as shown in Fig. 3. The flow rate decreases from 19.7 to 17.7 cc/min correspondingly, as seen in Fig. 4. It seems that the agreement between simulation and experiments is satisfactory.

4.2 Verification 2

Experimentally, Cheng [24] studied the alkali precipitate formation and its resultant permeability reduction with different hardness solutions when a strong base NaOH and a weak base Na_2CO_3 were injected. Experiments were made with Ottwa sand packed in stainless steel columns of 50 cm in length and 5 cm in radius. The initial permeability for the sample is 8.0–10.0 Darcy with 23 %–31 % porosity. The flow rate was

Table 4 Comparison between simulated results and laboratory test data

Case	Alkali type	Concentration of bivalent ion (ppm)		Permeability reduction (%)	
				Source data*	Our calculated results
1	NaOH	Ca^{2+}	1000	36	32.8
2	NaOH	Mg^{2+}	1000	55	49.6
3	NaOH	Ca^{2+}/Mg^{2+}	500/500	28	22.5
4	Na_2CO_3	Ca^{2+}	1000	12	9.7
5	Na_2CO_3	Mg^{2+}	1000	0	0
6	Na_2CO_3	Ca^{2+}/Mg^{2+}	500/500	18	13.4

* The source data come from reference [24]

Table 5 Reservoir description

Permeability (D)	1
Porosity	0.15
Initial oil pressure (Pa)	12×10^6
Temperature (°C)	50
Initial oil saturation	0.85
Initial oil sensity (kg/m^3)	800
Oil viscosity (Pa·s)	5×10^{-3}
Sandstone rock composition (%)	
Quartz	85.5
Feldspars	8.0
Clays	6.5

0.5–2.5 cc/min. The alkali concentration was 1.0 % Na_2O and the hardness level was either 500 or 1000 ppm of the divalent cation.

This experiment is also numerically simulated using our model. The comparison between simulation and Cheng's experiment shown in Table 4 is matched fairly well with reasonable errors. Numerical simulation also demonstrates that the permeability reduction can always be observed whether a strong base or a weak base was injected. Another important fact is that the degree of permeability reduction for a strong base is more severe than that of a weak base.

5 Results and discussion

With the model verified in the previous paragraph, 3D simulations of alkali migration are performed in a reservoir with characteristic parameters given in Table 5. With injection and a production well distance of 200 m and a reservoir thickness of 12 m, the simulations are conducted on a 1/4 well group of a 5-spot pattern, with 50 × 50 × 4 grids. Alkali agents include sodium hydroxide and sodium carbonate. In order to examine the migration of fluids expediently, we prefer to select the midpoint between injection and production wells as a target position in the reservoir.

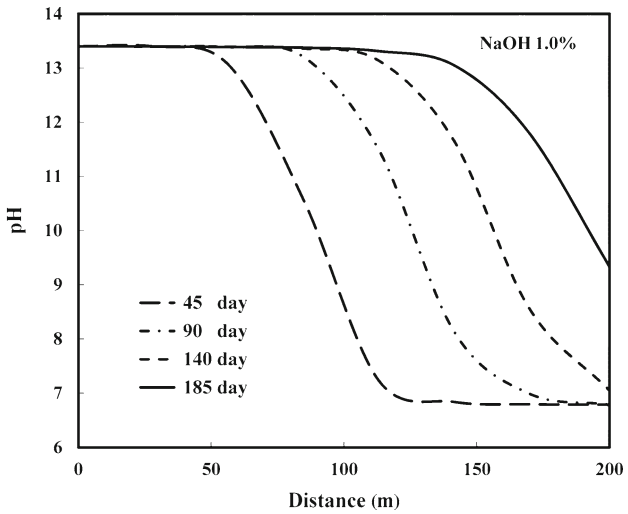

Fig. 5 pH value profiles during alkaline flooding *long dashed, dash dot, short dashed*, and *solid lines* represent results of 45, 90, 140, and 185 days, respectively)

5.1 Migration of alkaline solutions

The variation of pH value plays an important role in the process of alkaline flooding. Figure 5 shows the temporal and spatial evolution of pH value when 1.0 % NaOH solution is injected into the well. On the horizontal axis, zero point and point $x = 200$ stand for the injection and production wells, respectively. At the initial moment, the pH value almost remained at a neutral level of 6.8 all over the reservoir besides the injection well. The pH value of the injection well always maintains at 13.4 during the whole flooding process. With the transportation of flooding solution from injection to the production well, the pH value next to the injection well is increasing step by step as shown in Fig. 5. The temporal evolution of pH value can be seen by examining the variation of pH value somewhere in the stratum. The pH values at $x = 150$ m still maintain the initial value 6.8 when the displacement lasts for 45 days. This means that the sodium hydroxide solutions have not yet reached the place. With the

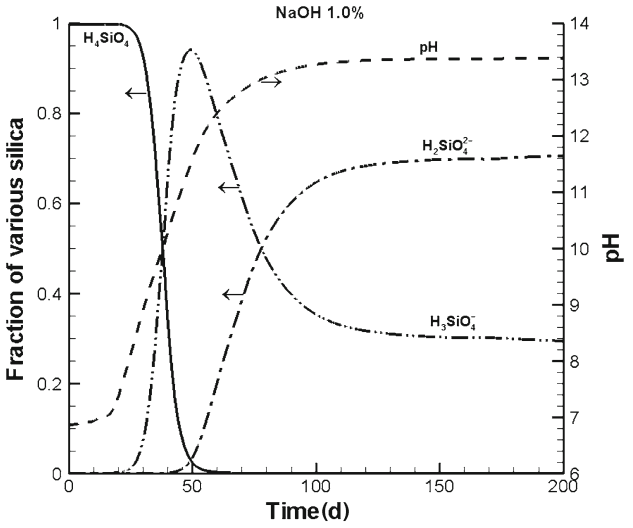

Fig. 6 Soluble silica speciation variation during the displacement process at target position in the reservoir (*dashed line* is pH value, *solid, double dot dash*, *dash dot line* are the H_4SiO_4, $H_3SiO_4^-$, $H_2SiO_4^{2-}$, respectively)

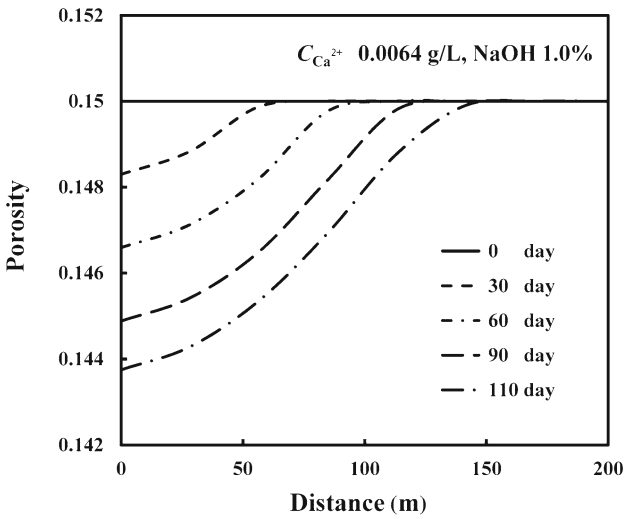

Fig. 7 Porosity variation profile from injection well to production well during the displacement process in the reservoir, caused by hydroxide scales

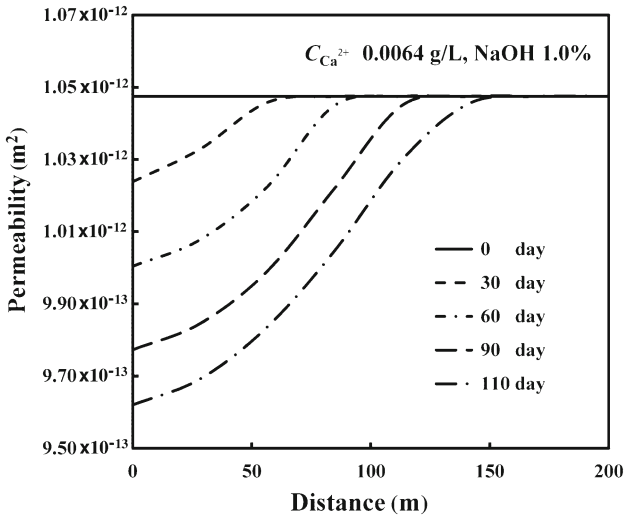

Fig. 8 Permeability variation profile from injection well to production well during the displacement process in the reservoir, caused by hydroxide scales

arrival of injected solution, the pH value starts to grow gradually.

5.2 Dissolution of quartz

As mentioned above, the solid silica contained in the reservoir rock is dissolved into the aqueous phase as a material source for the formation of scale. The dissolved silica mainly exists in various forms of amorphous silicon, such as H_4SiO_4, $H_3SiO_4^-$, $H_2SiO_4^{2-}$. Experiments show that the proportions of various amorphous silica vary with pH value [40–42]. Figure 6 exhibits the variations of various forms of amorphous silica at a target position in the reservoir when 1.0 % NaOH solution is injected. With the pH value increasing, the proportion of H_4SiO_4 rapidly decreases. In contrast, the proportion of $H_3SiO_4^-$ firstly increases to a maximum and then decreases. A monotonic increase in the proportion of $H_2SiO_4^{2-}$ occurs with pH values. When the pH value tends to a constant of 13.6, the fractions of various forms of amorphous silica reach a plateau.

5.3 Hydroxide scales

During the alkaline displacement process, when the ion product of calcium ions and hydroxide ions is greater than their solubility product, calcium hydroxide begins to precipitate. The precipitation deposits in the porous media, resulting in the reduction of pore diameter and, thus, porosity and permeability of the reservoir. Equations (11) and (12) are applied to calculate the reduction of porosity and pore radius. Then permeability can be obtained using the Eq. (8). So the deposition, which possibly does harm to the stratum, is undesirable.

Figures 7 and 8 demonstrate the effect of calcium hydroxide precipitation on the porosity and permeability in the reservoir. Due to the pH value at the injection well being higher, which has been discussed in the above section, the concentration of OH^- near the injection well is higher than elsewhere. So the ion product of calcium ions and hydroxide ions preferentially reaches the solubility product and the calcium hydroxide scaling mainly deposit at the injection well. Accordingly, the pore radius and porosity is reduced. With the displacement process from injection to the production well, the pH value next to the production well gradually

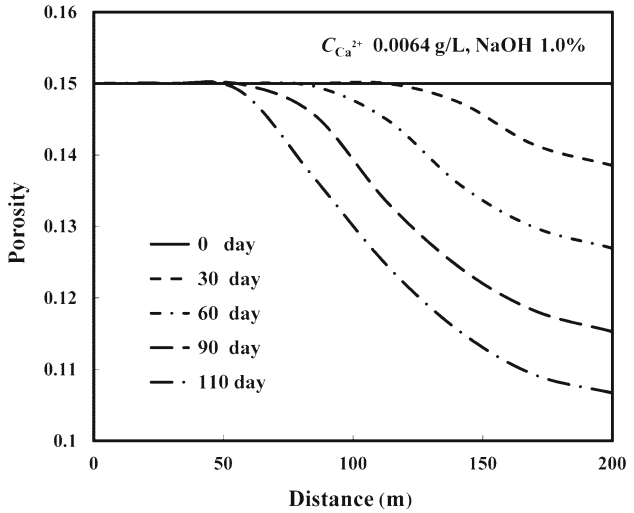

Fig. 9 Porosity variation profile from injection well to production well during the displacement process in the reservoir, caused by silicate scales

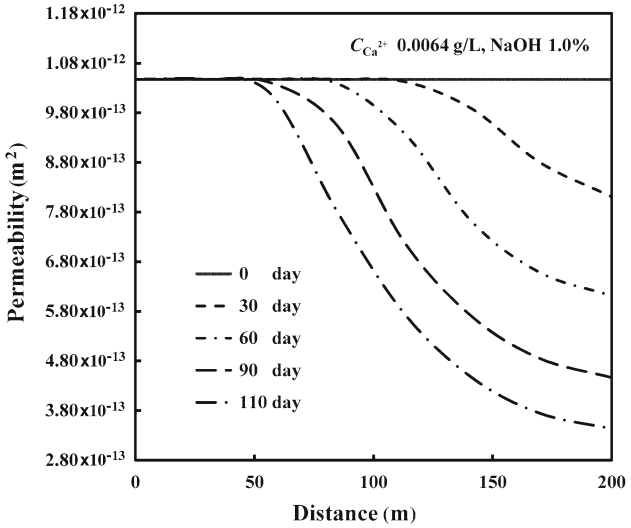

Fig. 10 Permeability variation profile from injection well to production well during the displacement process in the reservoir, caused by silicate scales

increases, the scaling gradually occurs in these places. The farther away from the injection well, the reduction degree of stratum parameters are smaller.

5.4 Silicate scales

The alkali agents can react with the reservoir rock to form dissolved silica, which exist in the form of amorphous silica in aqueous phase and the amorphous silica can precipitate with most multivalent metal cations. The slowly dissolved amorphous silica migrates with the displacement of fluid. Eventually the amorphous silica enrich the area nearby the production well. The amorphous silica concentration next to the production well is higher. When the concentration of amorphous silica reaches a certain degree, the ion product of silicate scales reaches the solubility product and silicate scales begin to deposit. With the displacement process, the amorphous silica continuously migrates forward and so the silicate scales gradually accumulate in the vicinity of the production well. Figures 9 and 10 describe the impact of silicate scales on the porosity and permeability in the reservoir. It is shown that the silicate scales have a great impact on the porosity and permeability nearby the production well and both of them decrease with the displacement process.

5.5 Calcium ion influence

Table 6 shows the effect of calcium ion concentration on the permeability reduction in different cases. It is found that whether a strong base or a weak base is used and regardless of their concentrations, the degree of permeability reduction is enhanced with the increasing of calcium ion concentration. For example, if 1.0 % NaOH solution is used, the permeability ratio after a month is 0.898 when the concentration of calcium ion is 0.25 g/L. When the calcium ion concentration is 0.08 g/L, the permeability ratio after a month is 0.942. If the calcium ion concentration is as low as 0.0064 g/L, the permeability ratio after a month is 0.973, shown in Table 6. So the effect of calcium ion concentration on the permeability reduction is apparent and lowering the calcium ion concentration seems to be helpful to alleviate scaling. Therefore, the calcium ion content in the water should be controlled in the injection water. Another result is that when a weak base is used, almost no scaling or only a small amount scaling is found in the simulation. When the concentration of Na_2CO_3 solution is 3.0 %, no scaling formed after a month. If its concentration is increased to 5.0 %, only a small amount alkali scaling formed and the permeability ratio after a month is 0.995. We can say the alkaline flooding of a weak base tends to inhibit the formation of alkali scales.

5.6 Effect of pressure and temperature on alkali scales

Many different variables, including temperature, pressure, ionic strength and salinity, may affect the scale precipitation [9,16,43]. Figures 11 and 12, respectively, show the impact of temperature and injection pressure on the permeability reduction at the production well. Results show the permeability decreases sharply, then slows down and eventually levels out during the migration process. This phenomenon was previously reported by Todd et al. [44] and Moghadasi et al. [45].

In order to research the effect of temperature on the permeability reduction, we executed simulation at different

Table 6 Effect of alkali concentration, calcium ion concentration on the permeability reduction, at production well

Case	Alkali concentration	Concentration of Ca^{2+} (g/L)	Precipitation amount after an hour (g/L)	Permeability ratio after a month	Permeability ratio after 3 month
1	0.15 % NaOH	0.25	84	0.947	0.845
2	0.50 % NaOH	0.25	124	0.922	0.776
3	1.00 % NaOH	0.25	164	0.898	0.710
4	1.00 % Na_2CO_3	0.25	12	0.992	0.977
5	3.00 % Na_2CO_3	0.25	68	0.957	0.874
6	5.00 % Na_2CO_3	0.25	87	0.945	0.840
7	0.15 % NaOH	0.08	13	0.992	0.975
8	0.50 % NaOH	0.08	63	0.960	0.883
9	1.00 % NaOH	0.08	92	0.942	0.831
10	1.00 % Na_2CO_3	0.08	–	–	–
11	3.00 % Na_2CO_3	0.08	–	–	0.984
12	5.00 % Na_2CO_3	0.08	8	0.995	0.985
13	1.00 % NaOH	0.0064	56	0.973	0.906

Note "–" indicates no precipitation

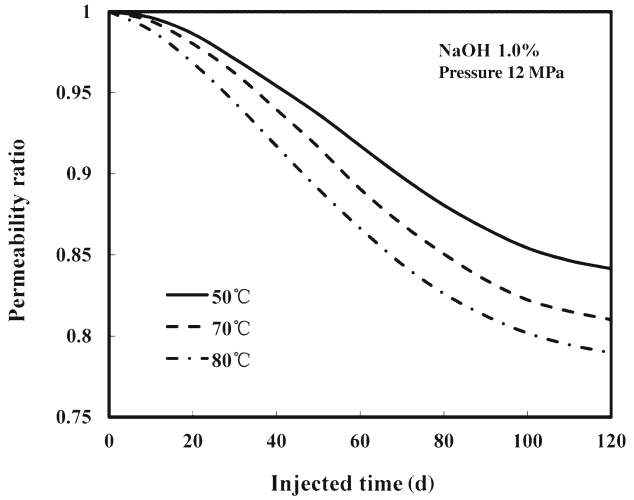

Fig. 11 The effect of temperature on permeability reduction, at the production well (*solid, dashed*, and *dash dot lines* represent results at temperature 50 °C, 70 °C, 80 °C, respectively)

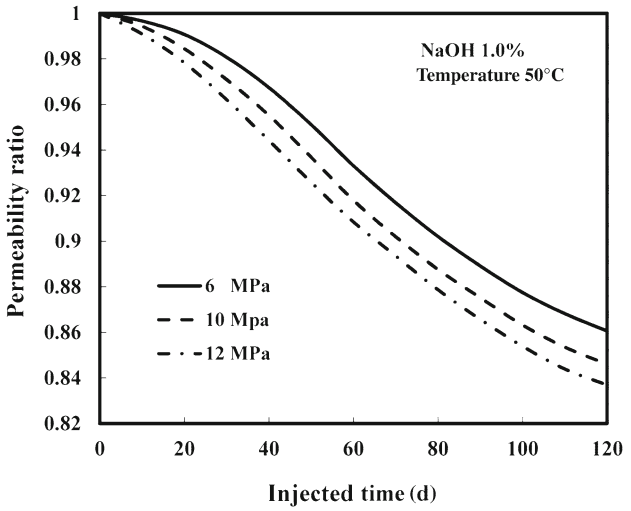

Fig. 12 The effect of pressure on permeability reduction, at the production well (*solid, dashed*, and *dash dot lines* represent results with injection pressure 6, 10, 12 MPa, respectively)

temperatures with the same pressure and ion concentration. Figure 11 shows the variation of the permeability reduction with flooding time at different temperatures. It can be seen that the permeability decreases more rapidly at higher temperature. Because of the dissolution of insoluble calcium compound, such as calcium carbonate, calcium hydroxide, they are accompanied by exotherm. The solubility product of insoluble calcium compounds decreases with the rise of temperature. The degree of supersaturation seems to be a driving force of precipitation reaction. Consequently, higher temperature leads to a larger scaling rate and a faster permeability reduction.

Let us turn to consider the effect of injection pressure on permeability reduction by numerical simulation at different pressures with the same temperature and ion concentration. Figure 12 shows that higher injection pressure also causes a larger permeability decline. Higher injection pressure leads to a higher injection rate, implying that more volume of flooding solution is injected into the reservoir at a given time interval. So the migration of ions is speeded up to quickly reach supersaturation state. Correspondingly, the rising precipitation rate causes a larger permeability reduction.

Temperature and pressure are two most significant factors affecting precipitation rate, we try to simulate a few

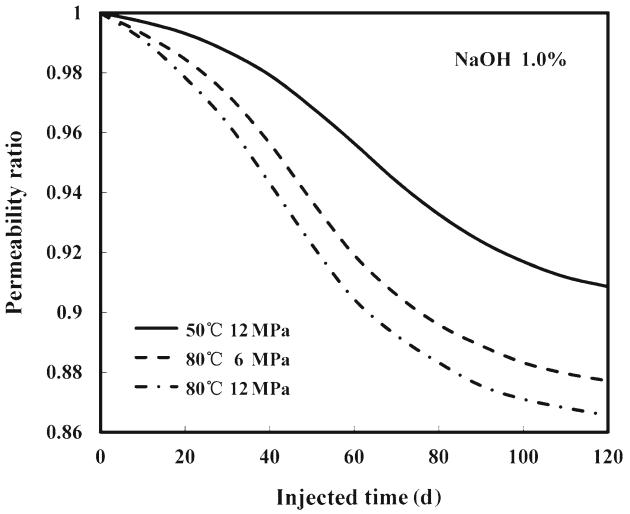

Fig. 13 Comparison of hydroxide scales under extreme conditions, at the injection well (*solid, dashed*, and *dash dot lines* represent high pressure, high temperature, high temperature and high pressure, respectively)

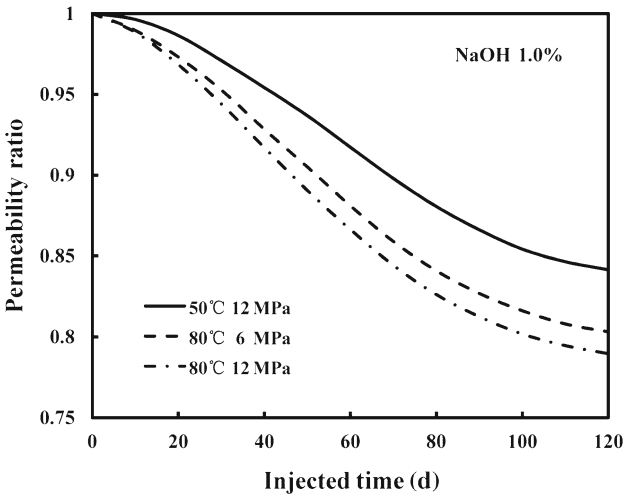

Fig. 14 Comparison of silicate scales under extreme conditions, at the production well (*solid, dashed*, and *dash dot lines* represent high pressure, high temperature, high temperature and high pressure, respectively)

extreme cases, namely high temperature, high pressure and both high temperature and high pressure. Since hydroxide scales mainly deposit nearby the injection well while silica scales precipitate around the production well, the minimum permeability ratio of the two kinds of scales cannot occur at the same place. Therefore, we only discuss the extreme cases for each kind of scales separately.

Figure 13 demonstrates the variation of permeability ratio at the injection well caused by hydroxide scales. Figure 14 demonstrates the variation of permeability ratio at the production well caused by silicate scales. Results show that the permeability is drastically reduced at both high temperature and high pressure. In particular, we notice that temperature exhibits a more remarkable influence on the permeability than pressure does.

5.7 Strong base versus weak base with different concentrations

Finally, we would study the effect of different types and concentrations of alkali on the oil recovery and precipitation, as listed in Table 7. It is found that the oil recovery increases with alkaline concentration whether a strong base or a weak base is injected. Herewith, a higher concentration of an alkali solution corresponding to higher concentration of hydroxide ion implies that more in-situ surface-active soap species can be produced. As a result, more residual oil will be emulsified and exploited. Furthermore, a permeability reduction can also be observed when the alkali agents are injected. The higher the alkali concentration is, the greater the reduction of permeability becomes.

A comparative analysis of the dissolution of the rock is shown in Fig. 15. When the same concentration of strong and weak base solutions are injected respectively, the concentration of amorphous silica with strong base is found an order of magnitude higher than that with weak base. In Table 8, simulated results show that oil recovery is only 3.2 % higher as 1.0 % NaOH and Na_2CO_3 is injected, respectively, while the degree of scaling tendency of a strong base is far more severe than that of a weak base. For comparison, we find that the injection of 1.0 % NaOH leads to a permeability reduction by 35 %, while injection of 1.0 % Na_2CO_3 only results in a permeability reduction by 2.8 % when 6 PV alkali solutions are injected into the reservoir, as shown in Table 9. So the degree of permeability reduction of a strong base is far more severe than that of a weak base.

5.8 Impacts of alkaline scales on stratum parameters and oil exploitation

Figures 16 and 17 describe the integrative spatio-temporal impact of alkaline scales on the porosity and permeability in the reservoir. The degree of reduction of porosity and permeability at the production well is the most severe in general. The closer the production well, the more severe the degree of reduction of reservoir parameters. Compared with the production well, the degree of reduction of porosity and permeability at the injection well is less severe. The porosity at the injection well and the production well are reduced to 95.9 % and 72 % of the original permeability, respectively. In the same way, the permeability at the injection well and production well are reduced to 91.4 % and 33.6 % of the original permeability, respectively. That means the scale deposition phenomenon near the production well is serious.

Table 7 Oil recovery and permeability reduction when NaOH and Na_2CO_3 injected, at the production well

Case	Alkali type	Concentration (%)	Injected pore volume (PV)	Oil recovery (%)	Permeability ratio (%)
1	NaOH	0.15	3.0	57.83	91
2	NaOH	0.15	6.0	69.74	83
3	NaOH	1.00	3.0	60.81	71
4	NaOH	1.00	6.0	71.96	65
5	Na_2CO_3	1.00	3.0	57.31	99.3
6	Na_2CO_3	1.00	6.0	68.76	97.2
7	Na_2CO_3	5.00	3.0	58.17	98.8
8	Na_2CO_3	5.00	6.0	68.95	95.7

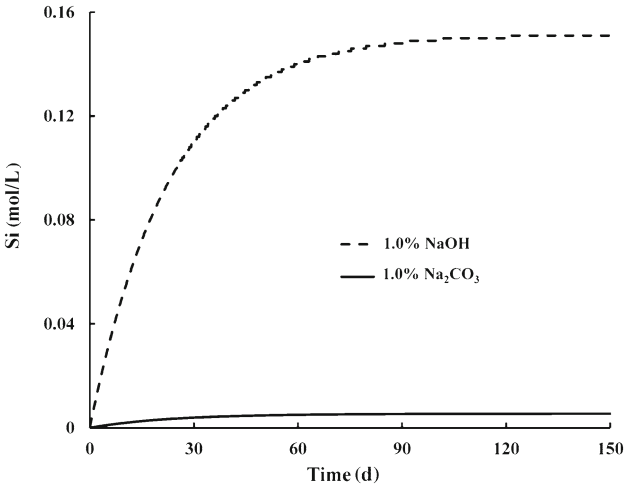

Fig. 15 Silica concentration when the same concentration of NaOH and Na_2CO_3 is injected, at the injection well

With the displacement process, the scales gradually deposit at the injection well and the injection pressure also rises. Figure 18 shows the temporal increase of injection pressure at the injection well. At the initial time the 14 MPa injection pressure is enough for the injection of displacement solution into the reservoir. As the injection process continues, the required injection pressure is increasing. After three months, the injection pressure increases from 14 to 15 MPa. That means the scale deposition phenomenon near the injection well can cause the increase of injection pressure.

Figure 19 shows the scale deposition at the production well can reduce the oil production. At the initial time the oil production rate is about 4.7 t/d. But with the exploitation process, the oil production falls sharply due to the formation of alkaline scales. After three months, the oil production rate reduces from 4.7 t/d to 2.0 t/d, accounting for 43 % of the initial production rate. So the scale deposition near the production well seriously impact the oil exploitation and measures should be taken to reduce these harmful impacts.

5.9 Application of this model in the Daqing oilfield

We apply this coupling model in the Daqing oilfield, where ASP flooding pilot tests were initiated as early as in 1982. Since 1993, three ASP pilot tests: West Central Block, Xing V Block, and West Block were implemented. Another two ASP industrial tests were put into production in Bei I Block and Xing II Block. These ASP pilot tests commenced after water flooding. Now the ASP flooding is becoming a dominant recovery technology in the Daqing oilfield. In order to recommend the feasible type of ASP flooding, the ASP

Table 8 Reservoir properties

	West central block	Xing V block	Xing II block
Permeability (D)	1.426	0.589	0.658
Porosity	0.26	0.23	0.26
Initial oil pressure (Pa)	10.93×10^6	11.65×10^6	11.18×10^6
Temperature (°C)	44.5	50.5	40.5
Initial oil saturation	0.748	0.65	0.65
Initial oil density (kg/m^3)	792	793	793
Oil viscosity (Pa·s)	9.5×10^{-3}	6.2×10^{-3}	6.5×10^{-3}
Concentration of Ca^{2+} (mg/L)	7.77	13.83	18.64
pH	8.3	8.23	7.8

Table 9 Comparison between field test data and simulation results

Case	Field test block	Alkali type	Concentration (%)	Field test		Simulation	
				EOR* (%)	Scaling level*	EOR (%)	Scaling level
1	Xing V block	NaOH	1.25	25.00	Serious	23.34	Serious
2	Xing II block	NaOH	1.20	23.24	Serious	20.60	Serious
3	West central block	Na_2CO_3	1.25	21.00	No	19.84	No
4	Xing II block	Na_2CO_3	1.60	24.60	No	21.56	No

* The field test data come from Ref. [11]

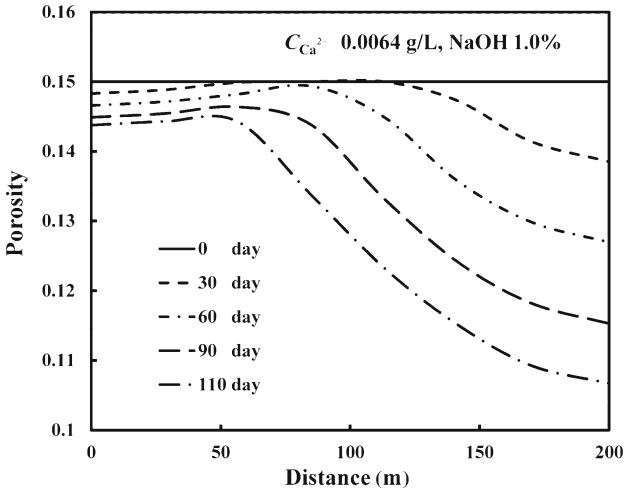

Fig. 16 Porosity variation profile from injection well to production well during the displacement process in the reservoir, caused by alkaline scales

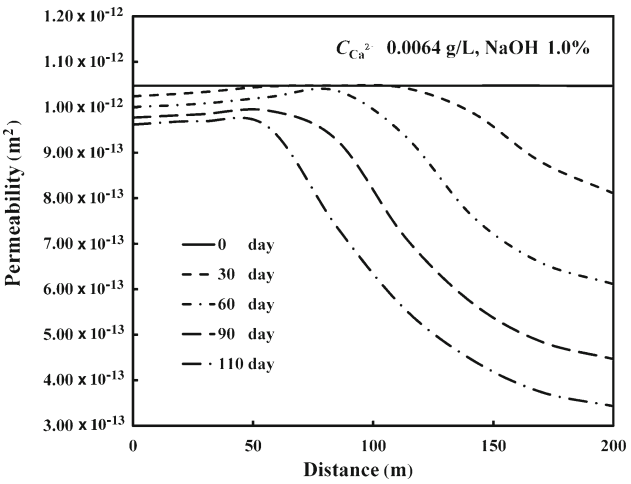

Fig. 17 Permeability variation profile from injection well to production well during the displacement process in the reservoir, caused by alkaline scales

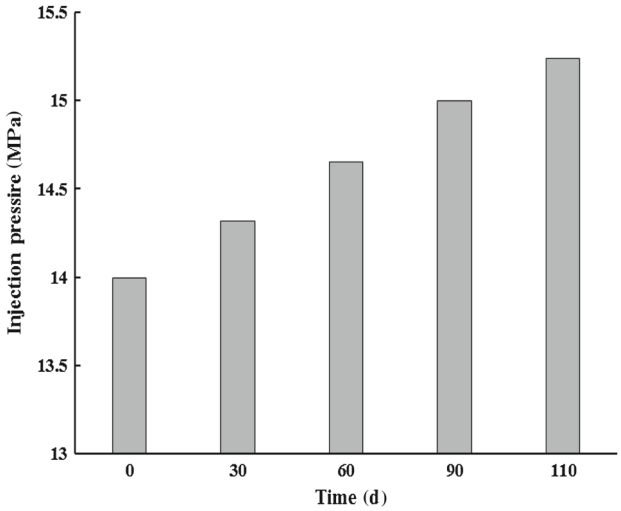

Fig. 18 Effect of alkaline scales on injection pressure

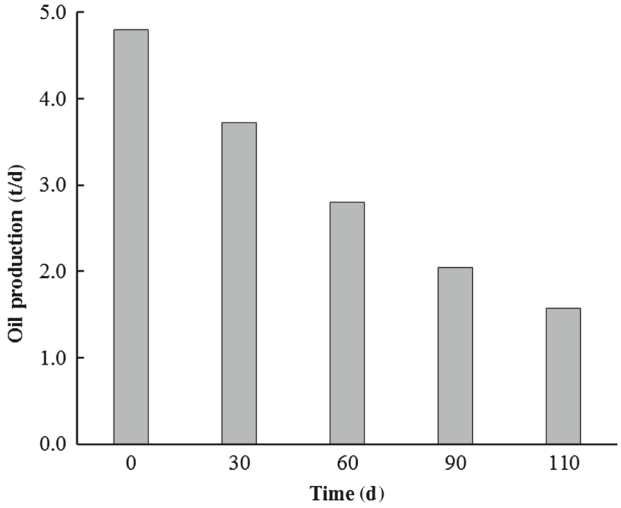

Fig. 19 Effect of alkaline scales on oil production

flooding with a weak base is compared with the ASP flooding with a strong base. We also choose the same alkalis in our simulation.

The reservoir properties of different simulation regions in the Daqing Oil field are given in Table 8. The simulations were conducted on a 1/4 well group of a 5-spot pattern. The comparison between field tests and simulation results are satisfactory as shown in Table 9. Scaling level is judged by the Ryznar index (RI) [46]. For instance, the scaling level is severe as RI is less than 5.0 and no scale occurs as RI is larger than 6.0. If the RI is between 5.0 and 6.0, the scaling level is light. The results demonstrated the oil recovery with

a strong base was slightly higher than with a weak base while the scaling levels were quite different. There were no scales at all when a weak base was used.

6 Conclusions

In the current study, we have established a comprehensive alkaline displacement model for a silica-based reservoir, considering various physicochemical phenomena involved in the alkaline flooding such as alkali/oil reactions, ion-exchange, rock dissolution, precipitation, and alkali loss. Especially as the coupling effects of scaling on porosity /permeability and seepage flow are considered in the model, the credibility of which has been verified by indoor lab experiments and in situ tests in the Daqing oilfield. According to the previous simulation and discussion on alkaline solution migration, quartz dissolution, scale movement and the effects of temperature, pressure and calcium ions, we can come to the following conclusions:

(1) During alkaline flooding, the solid silica contained in the reservoir rock is dissolved into the aqueous phase by injected alkali, then supplying material source for the formation of scales. The dissolved silica mainly exist in various forms of amorphous silicon, such as H_4SiO_4, $H_3SiO_4^-$, $H_2SiO_4^{2-}$. Since the first one is unstable in a high pH solution, then the proportion of silica species varies with pH values. With H_4SiO_4 vanished, $H_3SiO_4^-$ and $H_2SiO_4^{2-}$ finally reach a plateau of around 0.29 and 0.72, respectively, as the pH value monotonously rises to 13.4.

(2) We found that hydroxide scale deposits nearby the injection wells where the concentration of alkaline is the highest whereas silicate scales mainly precipitate adjacent to the production wells due to dissolved reactive product deposits there. The formation of scale may reduce pore diameter and porosity and permeability. The higher the alkali concentration, the greater the degree of permeability reduction. For instance, if 1.21 PV alkaline solutions are injected into the reservoir, 1.0 % Na_2CO_3 causes a minor influence on the permeability (reduced to 97.7 % of the original permeability). The effects of 0.15 % of NaOH and 5.0 % of Na_2CO_3 are equivalent (reduced to 94 % of the original permeability). And 1.0 % of NaOH results in a remarkable reduction in permeability (reduced to 71 % of the original permeability).

(3) The degree of reduction of porosity and permeability at the production well is the most severe for the whole reservoir in general. The closer the production well, the more severe the degree of reduction of reservoir parameters. The scale deposition at the injection well can cause the increase of injection pressure. The scale deposition at the production well can reduce the oil production.

(4) Temperature and injected pressure can drastically affect the precipitation. At higher temperatures, scaling is growing with the solubility of deposit decreasing, thus resulting in the decline of the permeability ratio as large as 5 % for 50 °C versus 80 °C. In the meantime, higher injected pressure also leads to a higher precipitation rate due to higher migration speed, and, thus, the difference of permeability rate reduction could be up to 2.2 % for 6 versus 12 MPa. Several extreme cases are simulated, showing that temperature has a more remarkable effect on the permeability than pressure.

(5) Calcium ions in injected water are prone to form alkali scaling. Simulation results reflect that the higher the calcium content, the easier the formation of precipitation. So injected water containing a low calcium ion concentration is preferable in the chemical flooding operation.

(6) Simulated results show that the improvement in EOR is only 3.2 as 1.0 % NaOH instead of 1.0 % Na_2CO_3 is injected. However, the concentration of soluble silica with a strong base is an order of magnitude higher than that with a weak base so that the stratum of the oil field could be severely damaged with its permeability reduced from 97.2 % to 65 %. So alkaline flooding of a weak base is strongly recommended in ASP chemical floods.

Acknowledgments The project was supported by the National Basic Research Program of China (Grant 2005CB221300) and the National Natural Science Foundation of China (Grant 11302234).

References

1. Fodi, B., Hentschke, R.: Simulated phase behavior of model surfactant solutions. Langmuir **16**, 1626–1633 (2000)
2. Liu, Q., Dong, M., Zhou, W., et al.: Improved oil recovery by adsorption-desorption in chemical flooding. J. Pet. Sci. Eng. **43**, 75–86 (2004)
3. Ratledge, C.: Fatty acid biosynthesis in microorganisms being used for single cell oil production. Biochimie **86**, 807–815 (2004)
4. Zhang, Z., Li, J.C., Zhou, J.F.: Microscopic roles of "viscoelasticity" in HPMA polymer flooding for EOR. Trans. Porous Media **86**, 229–244 (2011)
5. Okoye, C.U., Ping-Hu, W., Oungpasuk, P.: An improved linear chemical model for alkaline steamflooding. In: SPE Western Regional Meeting, Long Beach, 123–141 (1991)
6. Turksoy, U., Bagci, S.: Improved oil recovery using alkaline solutions in limestone medium. J. Pet. Sci. Eng. **26**, 105–119 (2000)
7. Chatterjee, J., Wasan, D.T.: A kinetic model for dynamic interfacial tension variation in an acidic oil/alkali/surfactant system. Chem. Eng. Sci. **53**, 2711–2725 (1998)
8. Efremov, E.P., Vachourkine, A.I.: A generalized statement concerning the results of laboratory and test studies on alkaline injection in an experimental area of the Trekhozernoye Deposit. In: European Symposium on EOR, Paris (1982)

9. Krumrine, P.H., Mayer, E.H., Brock, G.F.: Scale formation during alkaline flooding. J. Pet. Technol. **37**, 1466–1474 (1985)
10. Li, P., Cheng, Z.F., Wang, X.J.: Forming mechanism and prediction method of silica scaling in oil wells with alkaline-surfactant-polymer flooding. Acta Pet. Sin. **24**, 63–66 (2003). (in Chinese)
11. Zhao, C.J., Li, X.F., Zhou, S.H.: The scale analysis of ASP flooding in Daqing oil field. Pet. Geol. Recov. Effic. **13**, 93–95 (2006). (in Chinese)
12. Song, R., Xu, D.P., Zuo, X.W.: A case study of ASP multi-well groups. In: SPE EOR Conference at Oil & Gas West Asia, Muscat (2010)
13. Joseph, A., Kirk, M., Tyler, E.: Mitigating silicate scale in production wells in an oilfield in Alberta. In: SPE International Symposium on Oilfield Chemistry, The Woodlands (2011)
14. Liu, W.C., Yan, S.G., Jiang, B.N.: Alumosilicate scale formation owing to alkalis in chemical flooding solutionsIprecipitation of alumosilicates in alkali kaolinite systems. Oilfield Chem. **13**, 64–67 (1996). (in Chinese)
15. Abu-Khamsin, S.A., Ahmad, S.J.: Laboratory study on precipitation of calcium sulphate in Berea sandstone cores. In: SPE Technical Symposium of Saudi Arabia Section, Dhahran (2005)
16. Amer, B.M.: The study of scale formation in oil reservoir during water injection at high-barium and high-salinity formation water. [Master Thesis]. Universiti Teknologi Malaysia (2007)
17. Zhang, Q.S., Chen, W.: Scaling property and regularity of production well by ASP flooding process in Daqing oil field. Xinjiang Pet. Geol. **31**, 78–80 (2010). (in Chinese)
18. Sanford, W.E.: Simulation of calcite dissolution and porosity changes in saltwater mixing zones in coastal aquifers. Water Resour. Res. **25**, 655–667 (1989)
19. Le Gallo, Y., Bildstein, O., Brosse, E.: Coupled reaction-flow modeling of diagenetic changes in reservoir permeability, porosity and mineral compositions. J. Hydrol. **209**, 366–388 (1998)
20. Noiriel, C., Gouze, P., Bernard, D.: Investigation of porosity and permeability effects from microstructure changes during limestone dissolution. Geophys. Res. Lett. **31**, L24603 (2004)
21. Al Gahtani, F.: Diagenetic controls on evolution of porosity in the permian illawarra coal measures, Southern Sydney Basin, Australia. Arab. J. Geosci. **7**, 5473–5494 (2014)
22. Mohnot, S.M., Bae, J.H., Foley, W.L.: A study of mineral/alkali reactions. SPE Reserv. Eng. **2**, 653–663 (1987)
23. Shi, G.R.: Dissolution-precipitation model for smectite-illite transformation. Acta Pet. Sin. **27**, 47–50 (2006). (in Chinese)
24. Cheng, K.H.: Chemical consumption during alkaline flooding: A comparative evaluation. In: SPE/DOS Symposium on Enhanced Oil Recovery, Tulsa (1986)
25. Dezabala, E.F., Vislocky, J.M., Rubin, E.: A chemical theory for linear alkaline flooding. SPE J. **22**, 245–258 (1982)
26. Bunge, A.L., Radke, C.J.: Migration of alkaline pulses in reservoir sands. SPE J. **22**, 998–1012 (1982)
27. Ramakrishnan, T.S., Wasan, D.T.: Fractional-flow model for high-pH flooding. SPE Reserv. Eng. **4**, 59–68 (1989)
28. Bhuyan, D., Lake, L.W., Pope, G.A.: Mathematical modeling of high-pH chemical flooding. SPE Reserv. Eng. **5**, 213–220 (1990)
29. Labrid, J.C., Pierre, L.T.: A numerical model for predicting alkali slug migration in chemical processes. In: SPE/DOE Enhanced Oil Recovery Symposium, Tulsa (1992)
30. Li, X.B., Wu, S.H., Song, J.: Numerical simulation of pore-scale flow in chemical flooding process. Theor. Appl. Mech. Lett. **1**, 68–72 (2011)
31. Thornton, S.D., Radke, C.J.: Dissolution and condensation kinetics of silica in alkaline solution. SPE Res. Eng. **3**, 743–752 (1988)
32. O'Connor, T.L., Greenberg, S.A.: The kinetics for the solution of silica in aqueous solutions. J. Phys. Chem. **62**, 1195–1198 (1958)
33. Kozeny, J.: Über kapillare Leitung der Wasser in Boden. Sitzungs-Ber. Akad Wiss Wien **136**, 271–306 (1927). (in German)
34. Carman, P.: Fluid flow through a granular bed. Trans. Inst. Chem. Eng. **15**, 150–167 (1937)
35. Novosad, Z., Novosad, J.: Determination of alkalinity losses resulting from hydrogen-ion exchange in alkaline flooding. SPE J. **24**, 49–52 (1984)
36. Bazin, B., Labrid, J.: Ion exchange and dissolution/ precipitation modeling: application to the injection of aqueous fluids into a reservoir sandstone. SPE Reserv. Eng. **6**, 233–238 (1991)
37. Larson, R.G., Hirasaki, G.J.: Analysis of the physical mechanisms in surfactant flooding. SPE J. **18**, 42–58 (1978)
38. Yuan, S.Y., Yang, P.H.: A mathematical model of alkali combination flooding. Acta Pet. Sin. **15**, 76–88 (1994)
39. Satter, A., Shum, Y.M., Adams, W.T.: Chemical transport in porous media with dispersion and rate-controlled adsorption. SPE J. **20**, 129–138 (1980)
40. Ingri, N.: Equilibrium studies of polyanions, IV. silicate ions in NaCl medium. Acta Chem. Scand. **13**, 758–775 (1959)
41. Kopeykin, V.A., Mikhaylov, A.S.: Solubility and forms of occurrence of silica in normal dilute solutions. Doklady Academii Nauk SSSR **191**, 917–920 (1970)
42. Fleming, B.A., Crerar, D.A.: Silicic acid ionization and calculation of silica solubility at elevated temperature and pH. Geothermics **11**, 15–29 (1982)
43. Ma, C., Zhao, L., Zhan, C.C.: Mechanism, affecting factors and solution for silicate scale during alkaline flooding. West-China Explor. Eng. **3**, 95–96 (2006). (in Chinese)
44. Todd, A.C., Yuan, M.D., Heriot-Watt, U.: Barium and strontium sulfate solid-solution scale formation at elevated temperatures. SPE Prod. Eng. **7**, 85–92 (1992)
45. Moghadasi, J., Jamialahmadi, M., Müller-Steinhagen, H.: Scale formation in Iranian oil reservoir and production equipment during water injection. In: International Symposium on Oilfield Scale, Aberdeen (2003)
46. Cui, F.Y., Fang, Y., Yang, M., et al.: Prediction of inorganic scaling tendency due to injection of incompatible water in Chunjiu area of Shengli Oilfield. Earth Sci. Front. **19**, 301–306 (2012)